International Journal of Nanomedicine

Dovepress
open access to scientific and medical research

Open Access Full Text Article

ORIGINAL RESEARCH

Inhalable Nano-Dimpled Microspheres Containing Budesonide-PLGA for Improved Aerodynamic Performance

Chang-Soo Han[1,*], Ji-Hyun Kang[1,*], Young-Jin Kim[1], Dong-Wook Kim[2], Chun-Woong Park[1]

[1]College of Pharmacy, Chungbuk National University, Cheongju, 28160, Republic of Korea; [2]College of Pharmacy, Wonkwang University, Iksan, 54538, Republic of Korea

*These authors contributed equally to this work

Correspondence: Chun-Woong Park, College of Pharmacy, Chungbuk National University, 194-21, Osongsangmyeong 1-ro, Heungdeok-gu, Cheongju, Chungbuk, 28160, Republic of Korea, Tel +82-43-261-3330, Fax +82-43-268-2732, Email cwpark@cbnu.ac.kr

Introduction: Dry powder inhalations are an attractive pharmaceutical dosage form. They are environmentally friendly, portable, and physicochemical stable compared to other inhalation forms like pressurized metered-dose inhalers and nebulizers. Sufficient drug deposition of DPIs into the deep lung is required to enhance the therapeutic activity. Nanoscale surface roughness in microparticles could improve aerosolization and aerodynamic performance. This study aimed to prepare microspheres with nanoscale dimples and confirm the effect of roughness on inhalation efficiency.

Methods: The dimpled-surface on microspheres (MSs) was achieved by oil in water (O/W) emulsion-solvent evaporation by controlling the stirring rate. The physicochemical properties of MSs were characterized. Also, in vitro aerodynamic performance of MSs was evaluated by particle image velocimetry and computational fluid dynamics.

Results: The particle image velocimetry results showed that dimpled-surface MSs had better aerosolization, about 20% decreased X-axial velocity, and a variable angle, which could improve the aerodynamic performance. Furthermore, it was confirmed that the dimpled surface of MSs could cause movement away from the bronchial surface, which helps the MSs travel into the deep lung using computational fluid dynamics.

Conclusion: The dimpled-surface MSs showed a higher fine particle fraction value compared to smooth-surface MSs in the Andersen Cascade Impactor, and surface roughness like dimples on microspheres could improve aerosolization and lung deposition.

Keywords: nanoscale dimple, aerodynamic performance, particle image velocimetry, computational fluid dynamics

Introduction

Dry powder inhalers (DPIs) are attracting attention as treatments for lung diseases. DPIs have propellant-free, portable, and stable physicochemical properties and offer environmental and economic advantages. Successful therapy using DPIs depends upon the formulation, the aerosol device, and the patient.[1,2] This study investigated the effect of aerodynamic behavior on the dimpled nanostructure of microspheres. Microparticle roughness has been reported to have either a positive or a negative effect on pulmonary delivery. The negative effects of increased roughness were increased drug adhesion and particle-particle interaction in micro-level roughness.[3] In contrast, a positive effect was the reduction of particle-particle interactions due to nano-level roughness.[4–6] Furthermore, differences in surface roughness can also affect powder behavior in terms of particle velocity and the diversity of directions as it exits the device and moves within the lungs.[7,8] The dimpled structure and increased roughness of a golf ball allow for a four-times greater travel distance than does a smooth ball because of its reduced drag and lift. This causes the air to move faster at the top of the ball, creating a lower pressure there.[9,10] A dimpled nanostructure in microspheres can provide better aerodynamic behavior, similar to that of a golf ball. Increased roughness that does not have

Received: 28 April 2022
Accepted: 24 July 2022
Published: 3 August 2022

interlocking structures can show an improved aerodynamic performance owing to reduced particle-particle interactions and the behavior of the particles coming from the device and into the lungs.[11–14]

Dimpled microspheres have been prepared by a spray dryer, droplet imprinting, and the emulsion method.[15–17] The oil in water (O/W) solvent evaporation method is the simplest approach and obtains a high yield with a narrow particle size distribution.[18–20] Dimpled- surface and smooth-surface microspheres, consisting of budesonide (BUD) and poly (D, L lactic-co-glycolic acid) (PLGA) were made using the O/W solvent evaporation method.[21] We controlled for the shear rate in the solvent evaporation steps. They had similar sizes, distribution, and physicochemical properties, but different surface morphology.[22]

Particle image velocimetry (PIV) is a technique for capturing flow fields in fractions of a second. Particle characteristics such as velocity and direction can be quantified and analyzed in the obtained images. We confirmed the effect of the dimpled structure of the microparticles using a PIV system. Computational fluid dynamics (CFD) simulation is the study and calculation of fluid flow using computer simulations. CFD is a branch of fluid mechanics that uses numerical methods and algorithms for analyzing and resolving problems related to fluid flow.[23,24] The CFD method has recently been used to predict the behavior, distribution area, and deposited amount of inhalation formulation delivered via the pulmonary route.[25–27] The air velocity and pressure around the prepared MSs and their behavior within the bronchiolar walls were predicted.

This study prepared dimpled-surface microspheres and smooth-surface microspheres with BUD and PLGA using O/W solvent evaporation. The microspheres were evaluated to have similar size distribution, morphology, and physicochemical properties but different surface morphologies. We used atomic force microscopy to measure the depth of the dimples. We evaluated their aerodynamic performance using the Andersen Cascade Impactor and particle image velocimetry. Particle behavior on the bronchiolar surface was also predicted by CFD.

Materials and Method

Materials

Budesonide (BUD) was provided by INIST (Hwaseong-si, Korea). Poly (D, L lactic-co-glycolic acid) (PLGA) 503H was supplied by Evonik, Ltd. (Essen, Germany). Polyvinyl alcohol 500 (PVA 500) was purchased from the OCI Company, Ltd (Seoul, Korea). InhaLac 230 was provided by the Masung & CO Ltd. (Seoul, Korea). Methanol, dichloromethane (DCM), and acetonitrile (ACN) were high-performance liquid chromatography (HPLC) grades and purchased from Honeywell Burdick & Jackson Ltd. (Muskegon, MI, USA). Other chemicals were analytical grade and used as received. All experiments were carried out using Milli-Q distilled water.

Preparation of the Dimpled-Surface and Smooth-Surface Microspheres

Dimpled-surface MSs were prepared by O/W emulsion solvent evaporation as depicted in Figure 1. 500 mg PLGA 503H and 250 mg budesonide were dissolved in 25 mL dichloromethane methanol solution (9:1 v/v). They were placed into 500 mL of 0.2% polyvinyl alcohol at 1 mL/sec in a high-speed dispersion homogenizer (S18N-19G, IKA, Staufen, Germany) at 6000 rpm for 2 minutes to form an O/W emulsion. Next, we subjected the mixture to a different stirring rate with a mechanical stirrer (RW20 Digital, IKA, Staufen, Germany) in the range of 100 to 2000 rpm to dilute as shown in Table 1 and evaporate the solvent over 3 hours at 37 °C. The particles prepared at 100 rpm were named smooth-surface microspheres. The emulsion was first centrifuged at 500 rpm for 1 minute to eliminate the non-encapsulated budesonide particles and the resulting supernatant was collected. Next, the collected supernatant was centrifuged at 1500 rpm for 5 minutes. The smooth- and dimpled-surface microspheres were washed three times with distilled water before being collected using a 0.45 μm filter (Whatman, Clifton, NJ, USA) and distributed with 5 mL of distilled water. Finally, the smooth- and dimpled-surface microspheres were pretreated and lyophilized for two days at −50 °C. The prepared formulations were kept in a glass vial containing silica gel at −20 °C until used.

Morphology of Dimpled-Surface and Smooth-Surface Microspheres

We obtained scanning electron microscope (SEM) images of the dimpled-surface and smooth-surface MSs with the GEMINI LEO 1530 (Zeiss Ltd., Jena, Germany). The samples were mounted on an aluminum plate using carbon tape

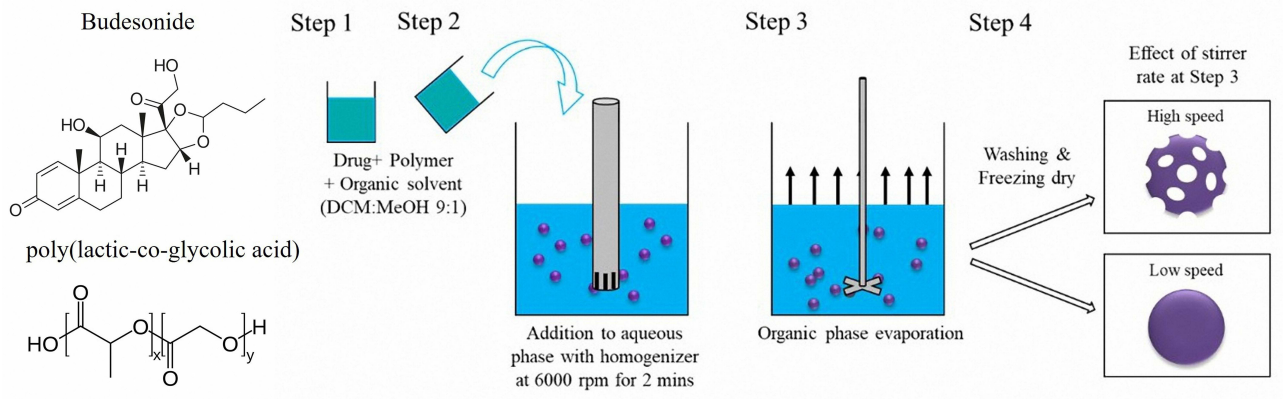

Figure 1 Schematic of preparing dimpled surface microspheres and chemical structure of budesonide and PLGA.

and the unattached particles were blown off. They were then placed inside a Hummer VI sputtering device (Minneapolis, MN, USA) and coated with a thickness of 200 Å platinum to discharge the particles. Magnifications were ×5000, ×10,000, and ×20,000. A voltage of 2 kV was applied.

Particle Size Distribution, Tapped Density, and Atomic Force Microscopy of Dimpled-Surface and Smooth-Surface Microspheres

The dimpled-surface and smooth-surface MSs were dispersed in distilled water for particle size distribution and measured using laser diffraction particle sizing (Mastersizer 3000, Malvern, Worcestershire, UK). The tapped density of the prepared formulations was measured using a 1-cc Luer-Lock syringe with a cap (BD Luer-Lok™, BD Bioscience, New Jersey, USA) and a linear scale with 0.01 mL increments. The syringe was filled with 100 mg of powdered sample and then tapped manually on a flat workbench until the volume remained constant. The volume was noted as the tapped volume and measured three times. Atomic force microscopy (AFM, Dimension Icon, Billerica, MA, USA) was used to analyze the surface topography of the prepared MSs. AFM images were acquired in the air by employing the conventional tapping mode. The samples were placed onto carbon tape and scanned using TESP-V2 cantilevers (Bruker). The images were captured with a scan size of 5 μm × 5 μm at a scan rate of 0.4 Hz. The images were analyzed using NanoScope Analysis 1.5 version software (Bruker). The root means square roughness (RMS) values were calculated from the AFM height deviation and the mean height value of each scan with the following equation (Equation 3).[28,29]

$$\mathrm{RMS} = \sqrt{\frac{h_1^2 + h_2^2 + h_3^2 + \ldots + h_n^2}{n}} \tag{3}$$

Physicochemical Properties of Dimpled-Surface and Smooth-Surface Microspheres

Differential Scanning Calorimeter

The thermal properties of the prepared MSs were analyzed using a Q2000 (TA Instruments Ltd., New Castle, DE, USA). The samples were heated from −10°C to 300°C at a rate of 10°C/min under a nitrogen flow of 50 mL/min.

Table 1 Preparation of Dimpled- and Smooth-Surface Microspheres. Effect of Mechanical Stirring Rate

Formulation	B5R100	B5R600	B5R1000	B5R2000
PLGA 503H (mg)	500	500	500	500
Budesonide (mg)	250	250	250	250
Mechanical stirring rate (rpm)	100	600	1000	2000

Powder X-Ray Diffraction

PXRD was performed under ambient conditions using X'Pert PRO MRD (PANalytical Ltd., Almelo, The Netherlands) with Cu Kα radiation generated at 40 mA and 40 kV. The samples were placed on a silicon plate at room temperature, and 2θ scans were collected from 5° to 60°.

Fourier-Transform Infrared Spectroscopy

Fourier-transform infrared (FT-IR) spectroscopy was performed on the prepared MSs in the range of 500 to 4000 cm^{-1} using a Cary 670 (Agilent, Santa Clara, CA, USA).

Encapsulation Efficiency and Drug-Loading Amount of Dimpled-Surface and Smooth-Surface Microspheres

The prepared B5R1000 and B5R100 formulations were selected as dimpled-surface and smooth-surface MSs. We measured their encapsulation efficiency with the validated HPLC method. The mobile phase was used acetonitrile and buffer (10mM sodium dihydrogen phosphate dihydrate and 10mM decane sulphonic acid) in a 6:4 (v/v) ratio. We dissolved 10 mg of the MSs in 50 mL of mobile phase solution using a Branson Model 8510 Ultrasonic Cleaner (BRANSON Ltd., St Louis, MO, USA) for 30 minutes. The analysis was performed with an Ultimate 3000 HPLC system (Thermo Scientific Ltd., Waltham, MA, USA) and a 5 μm, C18 column (100Å, 250 mm ×4.6 mm) from Phenomenex Ltd. (Torrance, CA, USA). The mobile phase was delivered at a flow rate of 0.5 mL/min. The detection wavelength was set at 222 nm, and the injection volume was 20 μL. The calibration curve was linear at a range from 1 to 100 μg/mL ($r^2 = 0.99997$). We calculated the entrapment efficiency (%) and drug loading (%) using equations Equations 1 and 2 as below, conducting all measurements in triplicate:

$$Encapsulation\ efficiency\ (\%) = \frac{Amount\ of\ drug\ in\ microspheres}{Theoretical\ amount\ of\ drug} \times 100 \quad (1)$$

$$Drug\ loading(\%) = \frac{Amount\ of\ drug\ encapsulated\ in\ microspheres}{Total\ amount\ of\ microspheres} \times 100 \quad (2)$$

Preparation of the Carrier-Based Formulations

The dimpled-carrier formulation and the smooth-carrier formulation were prepared by mixing the dimpled-surface and smooth-surface MSs with InhaLac 230 (1: 9 w/w). After the mixture was created, we analyzed the uniformity of the drug content in 50 mg samples at three positions (Top, middle, and bottom) using the Ultimate 3000 HPLC system with the same conditions as in Encapsulation Efficiency and Drug-Loading Amount of Dimpled-Surface and Smooth-Surface Microspheres.

Aerodynamic Performance of Carrier-Based Formulations

The aerosol performance of carrier-based formulations with the HandiHaler (Boehringer Ingelheim Pharmaceuticals, Inc, Ingelheim am Rhein, Germany) device was evaluated by using carrier-based formulations and an eight-stage nonviable Anderson cascade impactor (ACI) (TE-20-800, TISCH Environmental, Inc., Cleves, OH, USA) following the USP Chapter <601> specification for aerosols. A flow rate of 60 L/min was set and confirmed before each experiment using a flow meter (DFM 2000, COPLEY Scientific, Nottingham, UK). The ACI stage collection plates were coated with silicone oil to prevent particle bounce and re-entrainment during the test. Number 3 gelatin capsules were manually filled with 20 mg of each of the carrier-based formulations. A mouthpiece was mounted in the induction port, and the devices were inserted into that. The experiments were performed using a flow rate of 60 L/min for four seconds, and 20 capsules were used for each set of experiments. We quantified the amount of drug remaining in the capsules and distributed it onto the collection plate of each state using modified HPLC methods. We determined the aerodynamic cutoff diameters of each stage as 8.6 μm, 6.5 μm, 4.4 μm, 3.3 μm, 2.0 μm, 1.1 μm, 0.54 μm, and 0.25 μm for stages −1 to 6 at a flow rate of 60 L/min. The emitted dose (ED) was intended to be the percentage of the difference between the initial weight and the remaining weight of the drug in the capsule after aerosolization. The fine particle fraction (FPF) indicated the ability of the particles to reach the respirable region with an aerodynamic size of about 5.0 μm or less. The FPF is expressed as the proportion of drug amount collected at stages 1 through 6 in the ED based on the following equations (Equations 4 and 5):

$$\text{Emitted dose(ED)}\% = \frac{\text{The total dose in the capsule} - \text{Drug amount remaining in the capsule}}{\text{The total dose in capsules}} * 100 \quad (4)$$

$$\text{Fine particle fraction(FPF)}\% = \frac{\text{Total drug amount on stages1 through 6}}{\text{Emitted drug amount}} * 100 \quad (5)$$

The mass median aerodynamic diameter (MMAD) and geometric standard deviation (GSD) were calculated from the drug mass deposited in the ACI stages.

Particle Image Velocimetry of Dimpled-Surface and Smooth-Surface Microspheres

The PIV system is depicted in Figure 2. Number 3 gelatin capsules were filled with 15 mg of dimpled-surface and smooth-surface MSs. The HandiHaler (Boehringer Ingelheim Pharmaceuticals, Inc, Ingelheim am Rhein, Germany) device was mounted within a clear acrylic cube (200 × 200×200 mm). A flow rate of 60 L/min was formed using a vacuum pump. (Edwards, Lomma, Sweden) An 8-mV laser sheet beam (specification, 532 nm) was produced parallel to the device with a diode laser (LaserLab, Yongin, Korea). Particle behavior images were obtained at 8000 frames/second, and 640×480 pixels with a high-speed camera (HAS-D71M, DITECT Corporation, Tokyo, Japan) positioned perpendicular to the laser sheet plane. The chamber was divided into 50×50 grids, and the images were processed by PIV analysis software (Flownizer 2D, DITECT Corporation). Particle velocities were obtained in images between two frames using the combined algorithm of recursive cross-correlation.

Computational Fluid Dynamics of Dimpled-Surface and Smooth-Surface Microspheres

The behavior of the dimpled-surface and smooth-surface MSs on bronchial surfaces was investigated using three-dimensional computational models with commercial FLUENT CFD software (ANSYS V6.3.26). The geometry of the airflow channel was extracted, and the mesh in the domain was generated with Gambit 2.4.6. We analyzed the generation in 14 bronchioles, which are asthma sites, as well as the deep lung. The flow rate (7.875 cm^3/sec), diameter (0.71 mm), and length (1.57 mm) were designed based on the literature.[13,24,30] Dimpled-surface MSs, with a 4-μm diameter and 900-nm dimples, were designed as an icosahedron. Five inflation layers were applied to the dimpled wall for more accurate results. The density and viscosity of air were measured as 1.225 kg/m^3 and 1.784 e^{-5} kg/msec, respectively. The dimpled-surface MSs and spaces had computation meshes of 4.0×10^6 tetrahedral cells. The turbulent flow was described with the Reynolds-averaged Navier–Stokes (RANS) equation and was solved using the SIMPLE algorithm. The second-order upwind scheme was also used for the discretization of the momentum equation. For the three-dimensional transient flow, the continuity and momentum equations were defined as (Equations 6–8):

$$\frac{\partial \rho}{\partial t} + \frac{\partial}{\partial x_i}(\rho u_i) = 0 \quad (6)$$

$$\frac{\partial}{\partial t}(\rho u_i) + \frac{\partial}{\partial x_i}(\rho u_i u_j) = \frac{\partial P}{\partial x_i} + \frac{\partial \tau_{ij}}{\partial x_j} + \rho g_i + F_i \quad (7)$$

where s tensor (τ_{ij}) is given by

$$\tau_{ij} = \left[\mu\left(\frac{\partial u_i}{\partial x_j} + \frac{\partial u_j}{\partial x_i}\right)\right] \quad (8)$$

Where P is the static pressure; ρ is the density; t is the time; x_i and u_i are the position and velocity components, respectively; ρg_i is the gravitational force, and F_i is the external force. A turbulence model was also needed to describe the swirl flow motion and vortex. The k-ω turbulence model, which uses the turbulent kinetic energy and the specific dissipation rate in the vicinity of a wall, was selected for the modeling since it can express ω in a simple mathematical expression instead of a complex attenuation function. The equations related to the k-ω turbulence model were as follows in Equations 9–11:

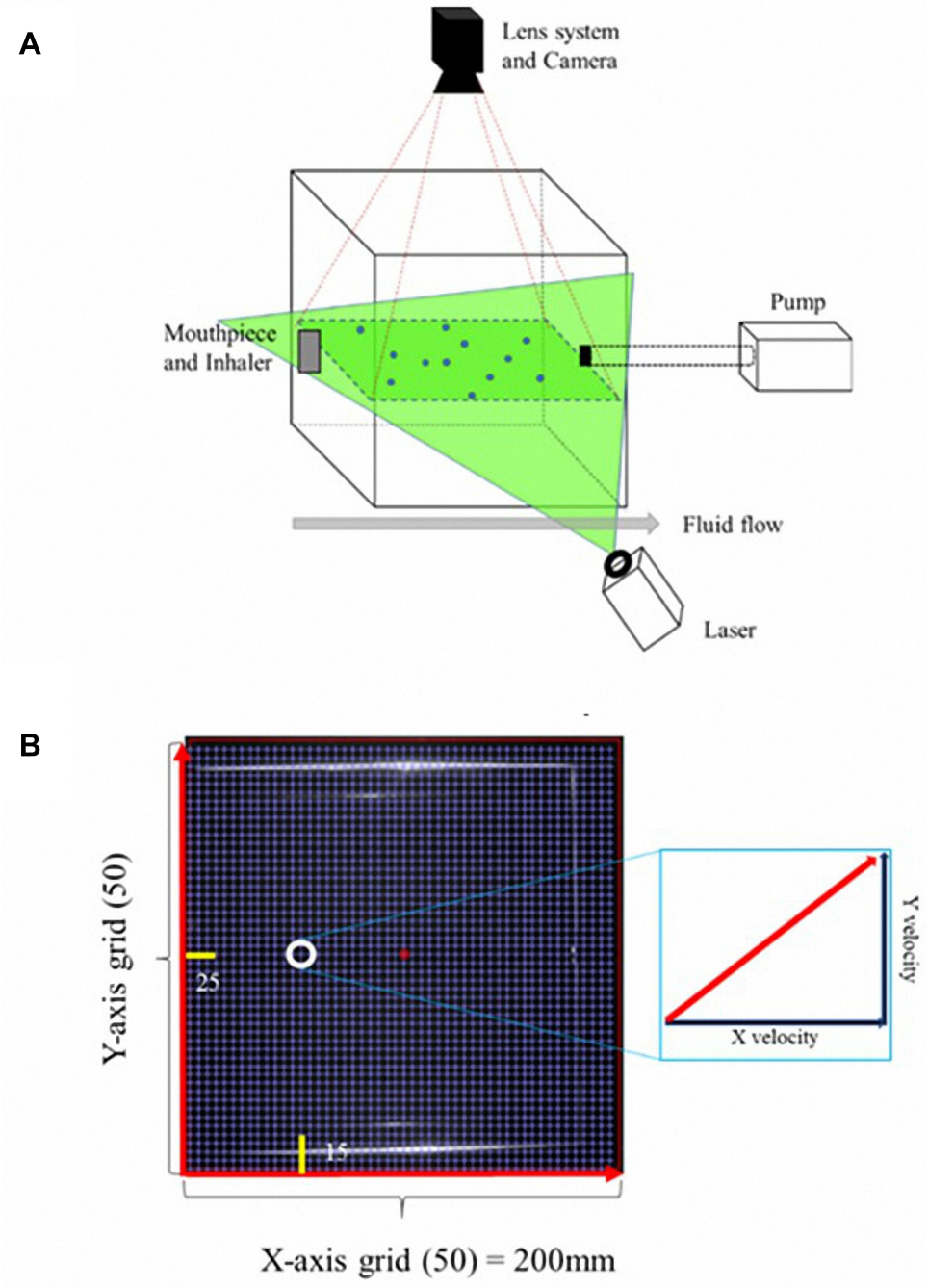

Figure 2 Particle image velocimetry. (**A**) Schematic of the PIV system and (**B**) grids of the PIV image for analysis.

$$\frac{\partial}{\partial t}(\rho k)+\frac{\partial}{\partial x_i}(\rho k u_i)=\frac{\partial}{\partial x_j}\left(\Gamma_k\frac{\partial k}{\partial x_j}\right)+\overline{G_k}-Y_k+S_k \tag{9}$$

$$\frac{\partial}{\partial t}(\rho \omega)+\frac{\partial}{\partial x_i}(\rho \omega u_i)=\frac{\partial}{\partial x_j}\left(\Gamma_\omega\frac{\partial \omega}{\partial x_j}\right)+G_\omega-Y_\omega+D_\omega+S_\omega \tag{10}$$

$$\Gamma_k=\mu+\frac{\mu_t}{\sigma_k},\Gamma_\omega=\mu+\frac{\mu_t}{\sigma_\omega} \tag{11}$$

In the equations, k represents the turbulence kinetic energy; ω the specific dissipation rate; G_k the turbulence kinetic energy generation owing to the average velocity gradient; G_ω the generation of the specific dissipation rate; and Y_k and Y_ω the extinction of k and ω, respectively, caused by turbulence. D_k is a cross-diffusion term; S_k and S_ω are source terms, and Γ is the turbulence diffusion coefficient. The flow rate and pressure changes around the prepared MSs were calculated according to the distance (3 μm, 6 μm, and 9 μm) from the bronchial wall. All of the output data were obtained from iterates that solved the process until the residual error reached 10^{-3}.

Statistical Analysis

All statistical analyses were conducted using the nested *t*-test using GraphPad Prism 8 (release 8.4.2, San Diego, CA, USA). *P*-values smaller than 0.05 were considered statistically significant.

Results and Discussion

Preparation of Dimpled-Surface and Smooth-Surface Microspheres

Budesonide-PLGA microspheres with dimpled-surface were prepared by O/W emulsion, which resulted in uniform particles. All prepared formulations were white powders. The SEM images of micronized BUD, PLGA 503H, and MSs prepared by different mechanical stirrer rates are shown in Figure 3. Micronized BUD was in an irregular, angular, and

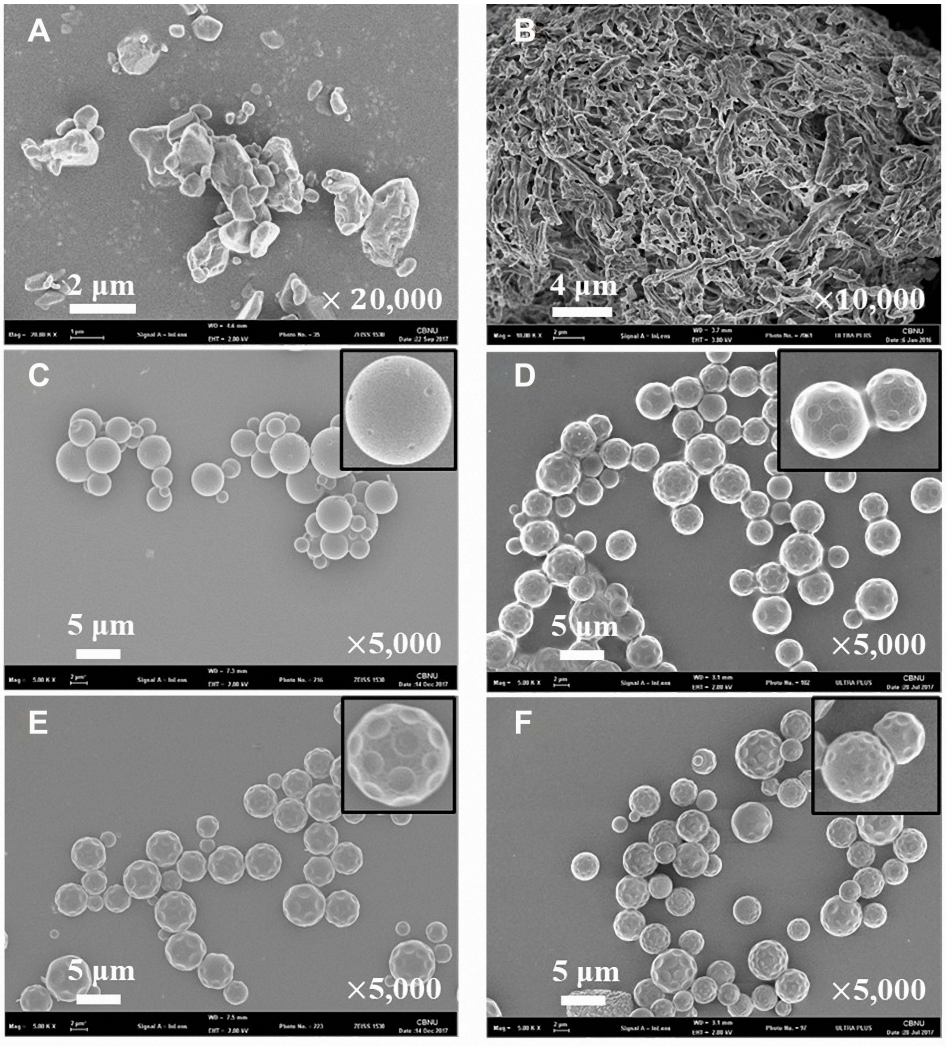

Figure 3 SEM micrographs of micronized budesonide, PLGA 503H, and microspheres according to mechanical stirring rate (**A**) Micronized budesonide (×20,000) (**B**) PLGA 503H (×10,000), (**C**) B5R100 (×5000), (**D**) B5R600 (×5000), (**E**) B5R1000 (×5000), and (**F**) B5R2000 (×5000).

crystalline form. PLGA 503H showed a fibrous morphology. The B5R100 showed sphere-shaped microsphere with smooth-surface. However, the B5R600, B5R1000, and B5R2000 were spherically shaped with dimpled-surfaces which could create by an increased solvent evaporation rate. B5R1000 had the most uniform dimpled-surface. But, in B5R600 and B5R2000, small and large dimples are mixed, and even within one particle, dimple-surface and smooth-surface are mixed. Rippled surfaces and air movement created by the high speed of a mechanical stirrer could provide an increased evaporation rate and fast shell formation.[31,32] The formation of the dimpled structure on microspheres is supposed to originate from crashes with smaller spheres. That evoked bulking effect during the solidification of PLGA particles.[16] It has a fast evaporation rate effect on the shell formation rate and increased collision in a small emulsion that creates dimpled-surfaces. However, an excessive or low rotational speed can cause uneven surface formation. The effect of the drug-polymer ratio and the evaporation rate by shear rate was confirmed. In this study, B5R100 and B5R1000 were chosen as models for smooth-surface MSs and dimpled-surface MSs, respectively.

Size Distribution, Tapped Density, and Surface Roughness of Dimpled-Surface and Smooth-Surface Microspheres

The particle size distribution of the prepared formulations is shown in Table 2. Prepared formulations had similar particle size distributions. The Dv_{50} value of the dimpled-surface MSs was 4.3 μm and that of the smooth-surface MSs was 4.7 μm. The measurements were in good agreement with the observations from the SEM images. The prepared formulations were observed to have similar tapped densities. The tapped density of the dimpled-surface MSs was 0.59 ± 0.05 g/cc and that of the smooth-surface MSs was 0.58 ± 0.01 g/cc. Since there is no significant difference in particle size and density, the difference in aerodynamic performance of dimple-surface MSs and smooth-surface MSs is derived from the surface structure. AFM images of the prepared MSs were taken and analyzed as in Figure 4. The depth of the dimples was about 186.4 ± 51.4 nm, and the RMS calculated by AFM was 192.0 nm. The smooth-surface MSs were not observed to have dimples. The nano-scaled dimples will be helpful to decrease particle-particle interactions and improve aerosolization.[33]

Physicochemical Properties of Dimpled-Surface and Smooth-Surface Microspheres

The DSC thermograms of the micronized BUD, PLGA 503H, the physical mixture of BUD and PLGA, the smooth-surface MSs, and the dimpled-surface MSs were obtained, and the results are shown in Figure 5A. The DSC results were obtained by raising the temperature 10 °C/min. The melting temperature (T_m) of micronized BUD was around 257°C.[34] In the case of PLGA 503H, the glass temperature (T_g) was observed at about 50°C, and the T_m was not observed. The physical mixture of BUD-PLGA503H, dimpled-surface MSs showed similar results. A little endothermic peak which was thought from BUD was observed around 225°C. Dimpled-surface MSs were thought to be in partial crystalline form. The smooth-surface MSs were similar to PLGA 503H which means an amorphous state.

Table 2 Particle Properties of Dimpled and Smooth-Surface Microspheres (n=3, Average ± Standard Deviation)

Sample	Dimpled MSs (B5R1000)	Smooth MSs (B5R100)
Dv10 (μm)	0.9	0.7
Dv50 (μm)	4.3	4.7
Dv90 (μm)	15.1	13.3
Span	3.272	2.634
Tapped density (g/cc)	0.59 ± 0.05	0.58 ± 0.01
Entrapment efficiency (%)	40.8 ± 1.6	13.5 ± 0.3
Drug loading amount (%)	13.6 ± 0.5	4.5 ± 0.1

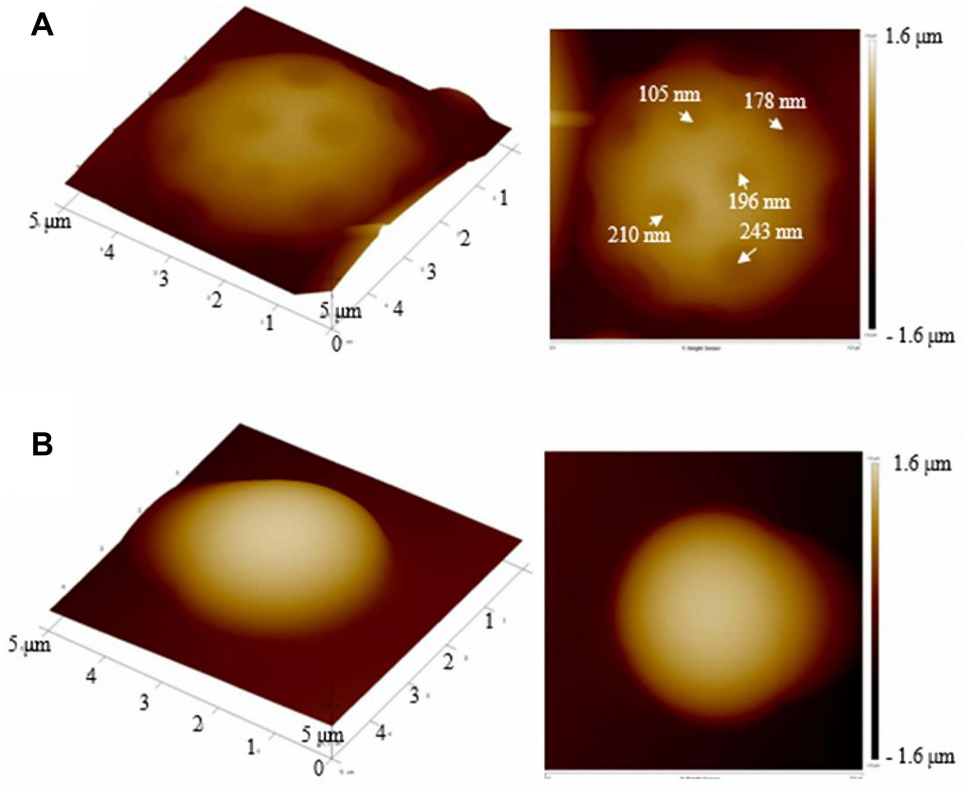

Figure 4 Atomic force microscopy images of the prepared formulations with root mean square values. (**A**) Dimpled-surface microsphere and (**B**) smooth-surface microsphere.

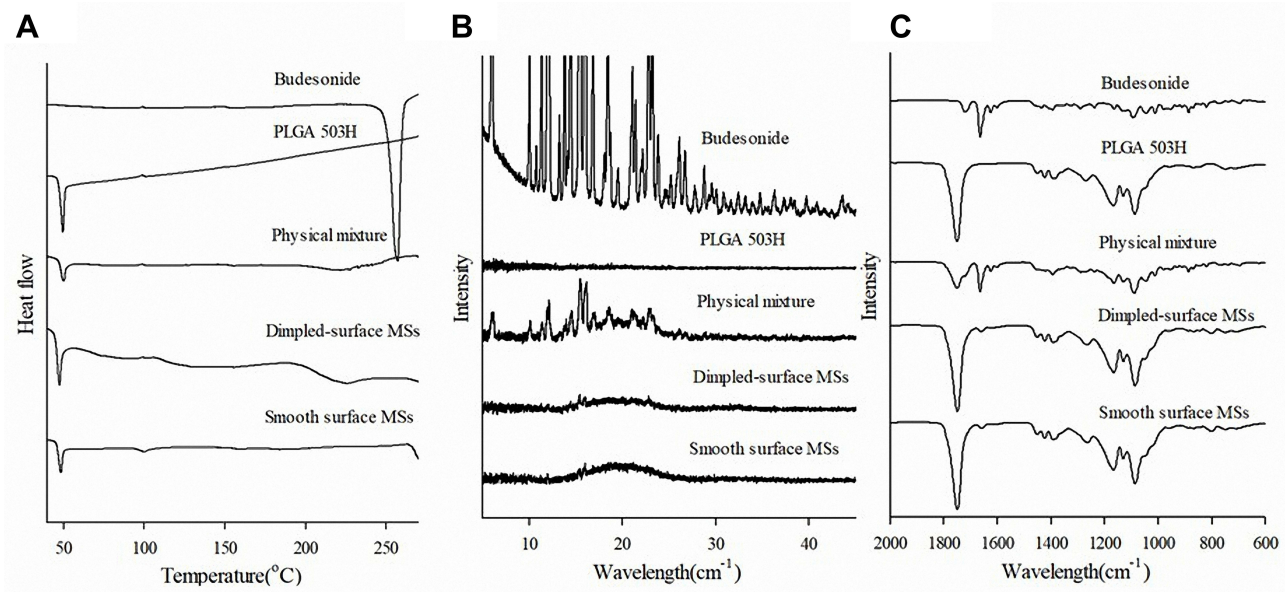

Figure 5 Physicochemical properties of dimpled and smooth-surface microspheres. (**A**) DSC results, (**B**) XRD results, and (**C**) FT-IR results.

The PXRD results are shown in Figure 5B. Sharp peaks were observed at around 6°, 12°, 15°, and 16° for BUD.[35] PLGA 503H was not observed to have a distinguished peak. The physical mixture showed a low-intensity BUD peak caused by the dilution effect of PLGA. Most dimpled-surface MSs were confirmed as having an amorphous form. However, small crystal peaks at 15°and 16° were observed that were thought to be small amounts of BUD on the surface

that had changed into a crystal form. The smooth-surface MSs were found to be amorphous. Comparing dimple- and smooth-surface MSs, the peak is a little higher because the BUD content is higher in the dimple-surface MSs with high loading efficiency (Table 2).

The FT-IR spectra of BUD, PLGA 503H, the physical mixture of BUD-PLGA, smooth-surface MSs, and dimpled-surface MSs are shown in Figure 5C. BUD had peaks at 1710 cm^{-1} (C = O bond), 1660 cm^{-1} (C = C bond), and 1100 cm^{-1} (C - O bond).[36] PLGA showed peaks at 1740 cm^{-1} (C = O bond), 1450–1350 cm^{-1} (C - C bond), and 1150–1050 cm^{-1} (C - O bond).[37] A BUD peak at 1660 cm^{-1} appeared in the physical mixture, smooth-surface MSs, and dimpled-surface MSs, but seemed to follow the PLGA 503H peak. The peak tendency of the prepared microspheres was like the physical mixture, which showed a tendency to depend upon the ratio between the drug and the polymer. The prepared MSs did not show a newly formed functional group.

Entrapment Efficiency and Drug Loading Amount of Dimpled-Surface and Smooth-Surface Microspheres

The results of entrapment efficiency, drug loading amount, and tapped density are presented in Table 2. The entrapment efficiency and drug loading amounts were measured by the validated HPLC method. In Table 2, the entrapment efficiency of the dimpled-surface MSs was estimated to be 40.8 ± 1.6%, and that of the smooth-surface MSs as 13.5 ± 0.3%. The drug loading amounts were 13.6 ± 0.5% and 4.5 ± 0.1%, respectively. The entrapment efficiency and drug loading amount differences between the dimpled-surface and smooth-surface MSs would be related to the rate of shell formation in the emulsion. A faster rate of stirring with the mechanical stirrer could accelerate emulsion solidification, and the rapid formation of PLGA microspheres would increase the drug entrapment efficiency of the dimpled-surface MSs.[38,39]

Aerodynamic Performance of Carrier-Based Formulations

The aerodynamic performance of the prepared formulations was evaluated using the Andersen Cascade Impactor with a HandiHaler DPI device. The ACI results are shown in Table 3. The prepared dimpled-surface and smooth-surface MSs exhibited 6.8 ± 0.2% and 7.6 ± 0.1% as mass median aerodynamic diameters (MMAD), 1.31 ± 0.0% and 1.2 ± 0.0% as geometric standard deviations (GSD), 82.3 ± 2.1% and 88.3 ± 1.5% as the ED, 11.0 ± 1.6% and 5.6 ± 0.4% as FPFs, and 44.1 ± 4.8% and 18.9 ± 2.1% as release fractions (RF), respectively. Since there is no significant difference in size and density (Table 2), the difference in MMAD is derived from the surface structure. According to FPF and RF values, dimpled-surface MSs had higher drug delivery efficiency than the smooth-surface MSs. The aerodynamic changes around the MSs with a dimpled-surface would positively affect the particles' travel as they enter the deep lungs.

Particle Image Velocimetry of Dimpled-Surface and Smooth-Surface MSs

Aerosolization of the dimpled-surface and smooth-surface MSs was measured by the PIV system. The capture images of them during 1000 frames are shown in Figure 6. Dimpled-surface MSs were observed with a wider area and spread angle than smooth-surface MSs. It is thought that aerosolization occurred better in dimpled-surface MSs due to reduced

Table 3 Aerodynamic Parameters of Dimpled and Smooth-Surface Microspheres (n=3, Average ± Standard Deviation)

Parameter	Dimpled MSs (B5R1000)	Smooth MSs (B5R100)
MMAD (μm)	6.8 ± 0.2	7.6 ± 0.1
GSD	1.31 ± 0.0	1.2 ± 0.0
ED (%)	82.3 ± 2.1	88.3 ± 1.5
FPF (%)	11.0 ± 1.6	5.6 ± 0.4
RF (%)	44.1 ± 4.8	18.9± 2.1

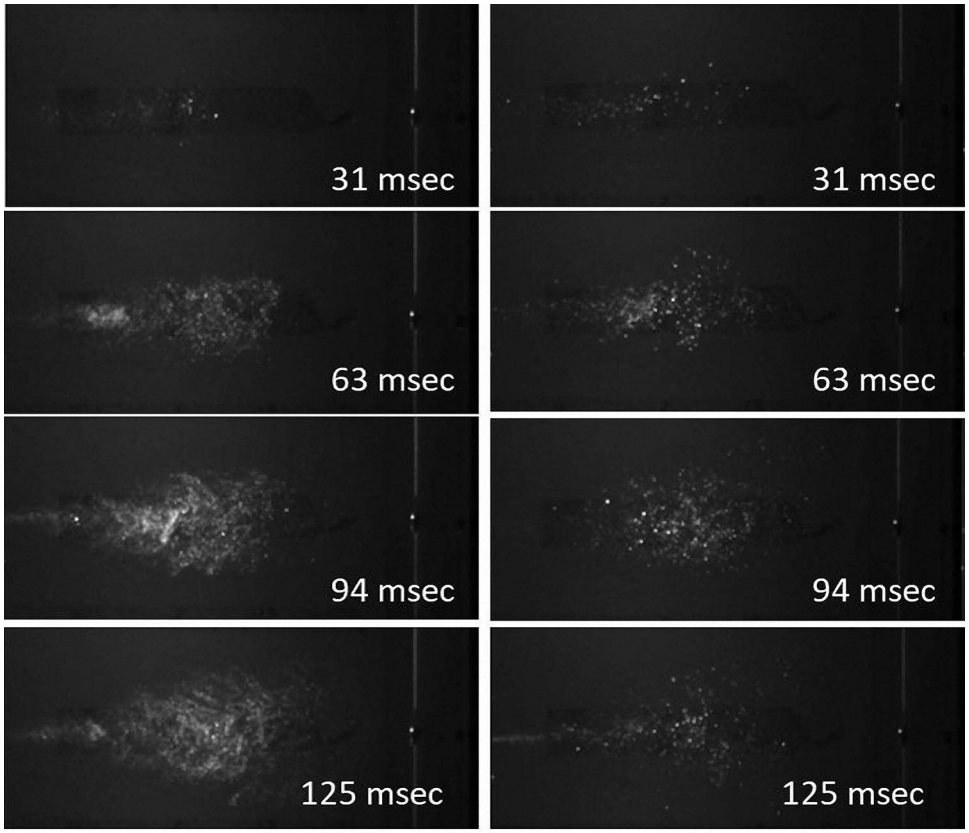

Figure 6 Captured images by PIV system at 31, 63, 94, 125 msec. (Left column) Dimpled-surface microspheres and (Right column) Smooth-surface microspheres.

particle-particle interaction due to the nanoscale dimpled structure.[11,40,41] These results are highly correlated with results of aerodynamic performance.

The grid,[15,24] representing the properties of the particles exiting the device, was analyzed in 0–1000 frames. The results are shown in Figure 7. The dimpled-surface MSs and smooth-surface MSs showed statistical differences in X-axial speed (dimple: 10.0 ± 3.9 mm/msec, smooth: 12.3 ± 4.5 mm/msec). The *p*-values were 0.02 by the nested *t*-test ($p < 0.05$). The Y-axial speed of the dimpled-surface MSs was 0.71 ± 0.43 mm/msec, and that of the smooth-surface MSs was 0.71 ± 0.43 mm/msec. The Y-axial speed was a very small value compared to the X-axial speed and would

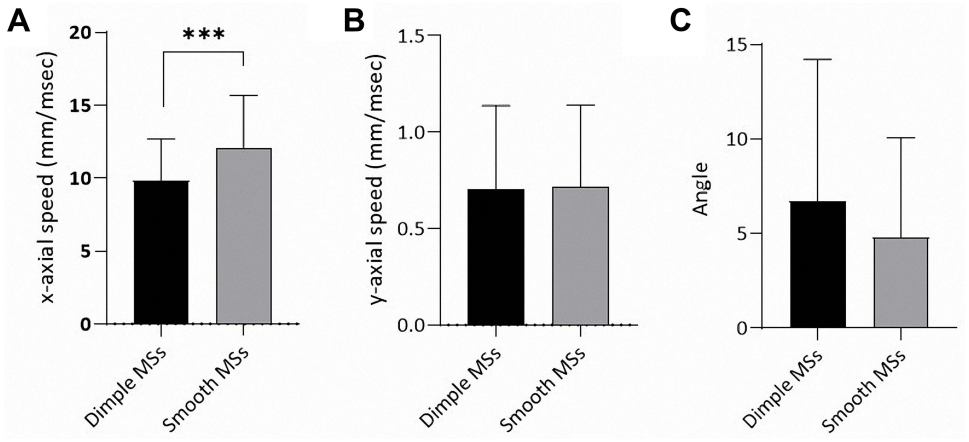

Figure 7 Results of particle image velocimetry at the grid[15,25] (n=3). (**A**) x-axial speed of dimpled- and smooth-surface microspheres, (**B**) y-axial speed of dimpled- and smooth-surface microspheres, and (**C**) angle of the dimpled- and smooth-surface microspheres (***Nested *t*-test, $p < 0.05$).

contribute less to the particle movement pattern. Although the *p*-value of the angle, indicating the diversity of the particle directions, was not enough to have a statistical difference of 0.06 ($p < 0.05$), the dimpled-surface MSs were observed to have a wider-angle distribution than the smooth-surface MSs. The roughness of the particle surface could affect the movement of the particle.[41] The dimpled structures on the prepared microparticles caused turbulence around the microparticles and various movements.[42] Decreased X-axial speed could reduce collisions in the throat. This is thought to improve the number of particles delivered to the lungs and increase diverse particle movement. It also helps to decrease loss at the throat during the administration of a DPI formulation.[43] Because of these characteristics, the dimple-surface MSs showed high efficiency in FPF and RF.

Computational Fluid Dynamics of Dimpled-Surface and Smooth-Surface MSs

The dimpled particles were designed through measured physical properties such as diameter and dimple depth and the particle movement in bronchioles was predicted using CFD. These results are highly correlated with in vitro aerodynamic performance tests and particle image velocimetry results. The designed particles and bronchioles are shown in Figure 8. When the designated particles were located 3 μm, 6 μm, and 9 μm from the wall, the fluid flow and pressure around the particles were calculated using CFD simulation. The results of the CFD simulation are shown in Figure 9. The side closer to the bronchial wall is described as the

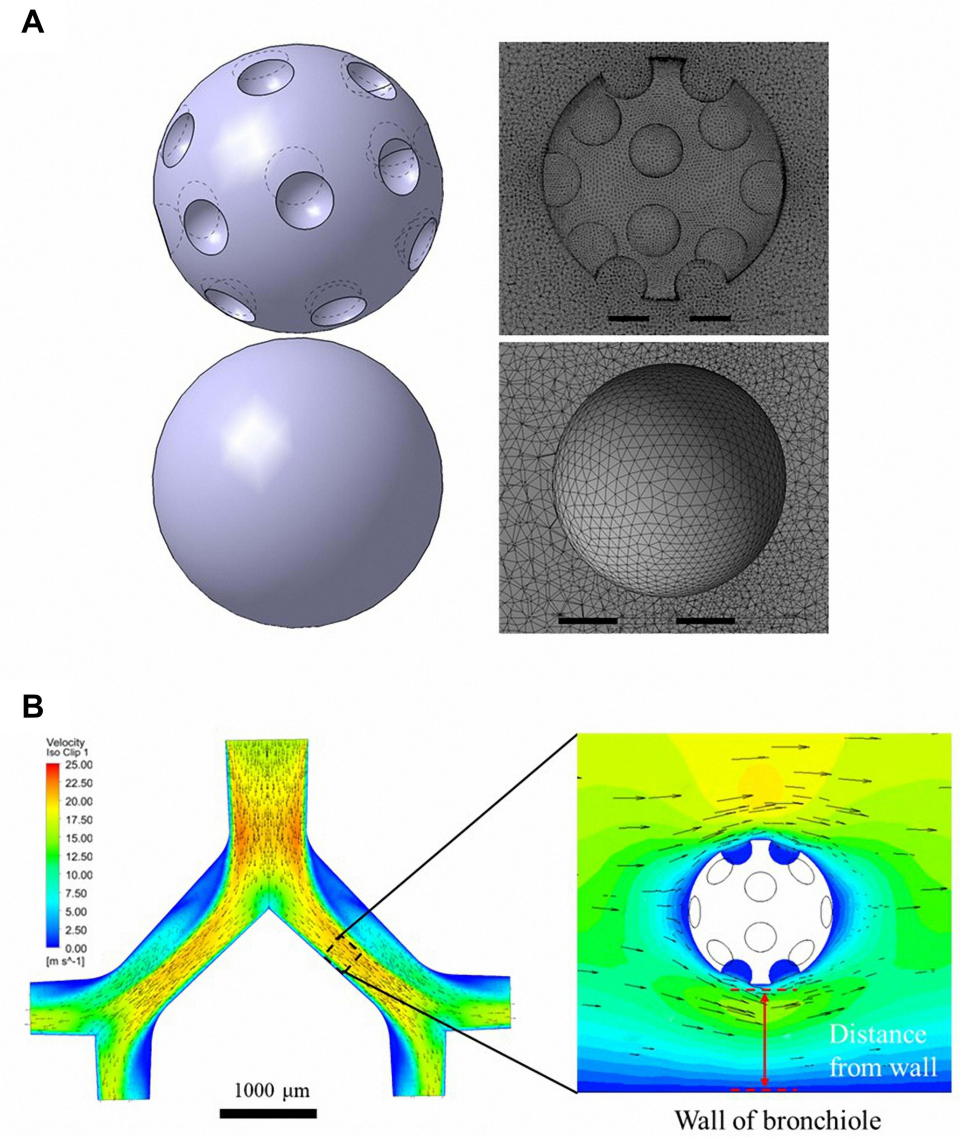

Figure 8 Simulation model. (**A**) Dimpled-surface microspheres design. (**B**) Bronchial design and microsphere positions in computational fluid dynamics.

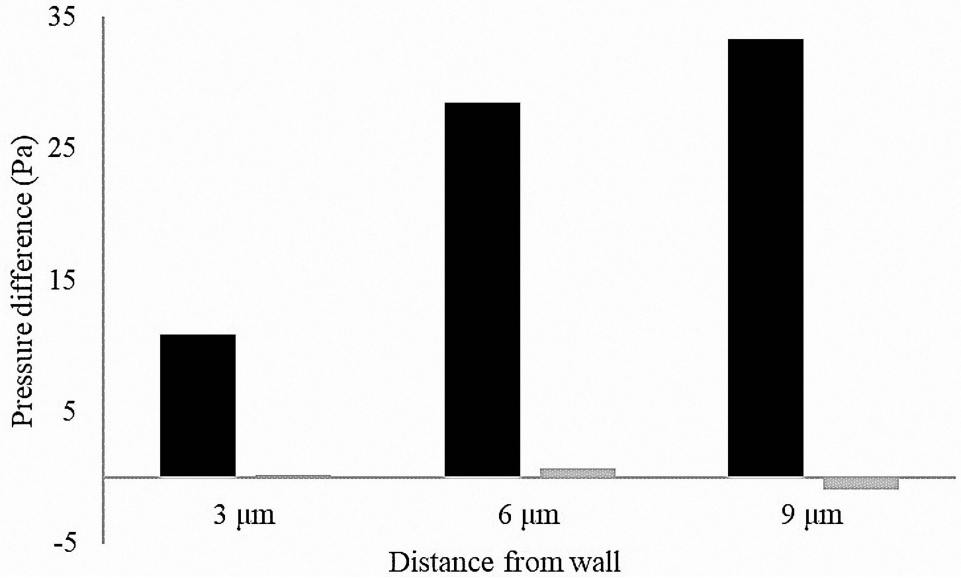

Figure 9 Simulation results: Pressure drop between the top and bottom of dimpled and smooth-surface microspheres (Black bar: dimpled-surface MSs, Grey bar: smooth-surface MSs).

bottom, and the side farther is called the top. The dimpled structures created eddies and affected the velocity flow around the MSs. Differences in the velocity flow between the top and bottom of the MSs were calculated and showed that the dimpled-surface MSs values were larger than those of the smooth-surface MSs at all distances from the wall. The pressure differences in the dimpled-surface MSs were 10.88 Pa, 28.49 Pa, and 33.33 Pa, depending upon the distance. Even in the case of smooth-surface MSs, the values increased with distance and appeared in the order of 0.23 Pa, 0.74 Pa, and 0.95 Pa. These pressure differences could cause the dimpled-surface MSs move away from the bronchial wall, which could avoid becoming attached to the wetted surfaces of the bronchioles and allowed them to travel deeper into the lungs.

Conclusion

Dimpled-surface MSs were prepared using O/W solvent evaporation, and B5R1000 was observed as having a uniform sphere shape with a dimpled-surface. The dimpled-surface and smooth-surface MSs had amorphous states and similar size distributions. The fact that dimpled- surfaces could enhance aerodynamic behavior has been demonstrated by ACI results such as the decreased MMAD and increased FPF and RF values. The CFD results also suggested that the dimpled structure on the microspheres could facilitate deep lung delivery of the drug by the flow changes around the microspheres caused by the dimples. Thus, in this study, we confirmed that a dimpled-surface on microspheres could improve the delivery of a drug deep into the lungs. However, the absolute inhalation efficiency has been observed as low, probably due to the electrostatic force of the polymers, capsules, and the device. These factors will need to be considered in further studies to prepare a more effective dry powder inhalation formulation.

Acknowledgments

This study was supported by a National Research Foundation of Korea grant provided by the Korean government (NRF-2018R1A1A1A05023012, NRF-2018R1D1A1B07050538, and 2017R1A5A2015541). This study was also supported by the Regional Innovation Strategy (RIS)" through the National Research Foundation of Korea (NRF) funded by the Ministry of Education (MOE). Finally, this work was financially supported by the Research Year of Chungbuk National University in 2022.

Disclosure

The authors report no conflicts of interest in this work.

References

1. Suarez S, Hickey AJ. Drug properties affecting aerosol behavior. *Respir Care*. 2000;45(6):652–666.
2. Peng T, Lin S, Niu B, et al. Influence of physical properties of carrier on the performance of dry powder inhalers. *Acta Pharm Sin B*. 2016;6(4):308–318. doi:10.1016/j.apsb.2016.03.011
3. Flament M-P, Leterme P, Gayot A. The influence of carrier roughness on adhesion, content uniformity and the in vitro deposition of terbutaline sulphate from dry powder inhalers. *Int J Pharm*. 2004;275(1–2):201–209. doi:10.1016/j.ijpharm.2004.02.002
4. Shalash AO, Molokhia AM, Elsayed MM. Biopharmaceutics. Insights into the roles of carrier microstructure in adhesive/carrier-based dry powder inhalation mixtures: carrier porosity and fine particle content. *Eur J Pharm Biopharm*. 2015;96:291–303. doi:10.1016/j.ejpb.2015.08.006
5. Lee JH, Lee C-S, Cho KY. Enhanced cell adhesion to the dimpled surfaces of golf-ball-shaped microparticles. *ACS Appl Mater Interfaces*. 2014;6(19):16493–16497. doi:10.1021/am505997s
6. Wang H, Nobes DS, Vehring R. Particle surface roughness improves colloidal stability of pressurized pharmaceutical suspensions. *Pharm Res*. 2019;36(3):43. doi:10.1007/s11095-019-2572-0
7. Adi S, Adi H, Tang P, Traini D, Chan H-K, Young PM. Micro-particle corrugation, adhesion and inhalation aerosol efficiency. *Eur J Pharm Sci*. 2008;35(1–2):12–18. doi:10.1016/j.ejps.2008.05.009
8. Kou X, Heng PW, Chan LW, Wereley ST, Carvajal MT. Effect of roughness on the dispersion of dry powders for inhalation: a dynamic visualization perspective. *AAPS PharmSciTech*. 2019;20(7):271. doi:10.1208/s12249-019-1482-0
9. Leong J-C, Lin C-Y. Effects of golf ball dimple configuration on aerodynamics, trajectory, and acoustics. *J Flow Vis Image Process*. 2007;14(2):43.
10. Libii JN. Dimples and drag: experimental demonstration of the aerodynamics of golf balls. *Am J Phys*. 2007;75(8):764–767. doi:10.1119/1.2673248
11. Peng T, Zhang X, Huang Y, et al. Nanoporous mannitol carrier prepared by non-organic solvent spray drying technique to enhance the aerosolization performance for dry powder inhalation. *Sci Rep*. 2017;7:46517. doi:10.1038/srep46517
12. Musante CJ, Schroeter JD, Rosati JA, Crowder TM, Hickey AJ, Martonen TB. Factors affecting the deposition of inhaled porous drug particles. *J Pharm Sci*. 2002;91(7):1590–1600. doi:10.1002/jps.10152
13. Nowak N, Kakade PP, Annapragada AV. Computational fluid dynamics simulation of airflow and aerosol deposition in human lungs. *Ann Biomed Eng*. 2003;31(4):374–390. doi:10.1114/1.1560632
14. Park H, Ha E-S, Kim M-S. Surface modification strategies for high-dose dry powder inhalers. *J Pharm Investig*. 2021;51:1–34.
15. Kim MR, Lim YT, Cho KY. Biodegradable microparticles with surface dimples as a bi-modal imaging contrast agent. *Macromol Rapid Commun*. 2013;34(5):406–410. doi:10.1002/marc.201200729
16. Qiao F, Zhang J, Wang J, et al. Silk fibroin-coated PLGA dimpled microspheres for retarded release of simvastatin. *Colloids Surf B*. 2017;158:112–118. doi:10.1016/j.colsurfb.2017.06.038
17. Emami F, Yazdi SJM, Na DH. Poly (lactic acid)/poly (lactic-co-glycolic acid) particulate carriers for pulmonary drug delivery. *J Pharm Investig*. 2019;49:1–16.
18. Li M, Rouaud O, Poncelet D. Microencapsulation by solvent evaporation: state of the art for process engineering approaches. *Int J Pharm*. 2008;363(1):26–39. doi:10.1016/j.ijpharm.2008.07.018
19. Sabliov C, Chen H, Yada R. *Nanotechnology and Functional Foods: Effective Delivery of Bioactive Ingredients*. John Wiley & Sons; 2015.
20. Lee WY, Asadujjaman M, Jee J-P. Long acting injectable formulations: the state of the arts and challenges of poly (lactic-co-glycolic acid) microsphere, hydrogel, organogel and liquid crystal. *J Pharm Investig*. 2019;49(4):459–476. doi:10.1007/s40005-019-00449-9
21. Schoubben A, Ricci M, Giovagnoli S. Meeting the unmet: from traditional to cutting-edge techniques for poly lactide and poly lactide-co-glycolide microparticle manufacturing. *J Pharm Investig*. 2019;49(4):381–404. doi:10.1007/s40005-019-00446-y
22. Park C-W, Lee H-J, Oh D-W, Kang J-H, Han C-S, Kim D-W. Preparation and in vitro/in vivo evaluation of PLGA microspheres containing norquetiapine for long-acting injection. *Drug Des Devel Ther*. 2018;12:711. doi:10.2147/DDDT.S151437
23. Tena AF, Clarà PC. Use of Computational fluid dynamics in respiratory medicine. *Archivos de Bronconeumología*. 2015;51(6):293–298. doi:10.1016/j.arbr.2015.03.005
24. de Boer AH, Hagedoorn P, Woolhouse R, Wynn E. Computational fluid dynamics (CFD) assisted performance evaluation of the Twincer™ disposable high-dose dry powder inhaler. *J Pharm Pharmacol*. 2012;64(9):1316–1325. doi:10.1111/j.2042-7158.2012.01511.x
25. Yousefi M, Pourmehran O, Gorji-Bandpy M, et al. CFD simulation of aerosol delivery to a human lung via surface acoustic wave nebulization. *Biomech Model Mechanobiol*. 2017;16(6):2035–2050. doi:10.1007/s10237-017-0936-0
26. Augusto L, Lopes G, Goncalves J. A CFD study of deposition of pharmaceutical aerosols under different respiratory conditions. *Braz J Chem Eng*. 2016;33(3):549–558. doi:10.1590/0104-6632.20160333s20150100
27. Lee H-G, Kim D-W, Park C-W. Dry powder inhaler for pulmonary drug delivery: human respiratory system, approved products and therapeutic equivalence guideline. *J Pharm Investig*. 2018;48(6):603–616. doi:10.1007/s40005-017-0359-z
28. Bhushan B. Surface roughness analysis and measurement techniques. In: *Modern Tribology Handbook, Two Volume Set*. CRC press; 2000:79–150.
29. Duparre A, Ferre-Borrull J, Gliech S, Notni G, Steinert J, Bennett JM. Surface characterization techniques for determining the root-mean-square roughness and power spectral densities of optical components. *Appl Opt*. 2002;41(1):154–171. doi:10.1364/AO.41.000154
30. Sul B, Wallqvist A, Morris MJ, Reifman J, Rakesh V. Medicine. A computational study of the respiratory airflow characteristics in normal and obstructed human airways. *Comput Biol Med*. 2014;52:130–143. doi:10.1016/j.compbiomed.2014.06.008
31. Poós T, Varju E. Review for prediction of evaporation rate at natural convection. *Heat Mass Transfer*. 2019;55(6):1651–1660. doi:10.1007/s00231-018-02535-4
32. Liggins RT, Burt HM. Paclitaxel loaded poly (L-lactic acid)(PLLA) microspheres: II. The effect of processing parameters on microsphere morphology and drug release kinetics. *Int J Pharm*. 2004;281(1–2):103–106. doi:10.1016/j.ijpharm.2004.05.027
33. Renner N, Steckel H, Urbanetz N, Scherließ R. Nano-and Microstructured model carrier surfaces to alter dry powder inhaler performance. *Int J Pharm*. 2017;518(1–2):20–28. doi:10.1016/j.ijpharm.2016.12.052
34. Goyanes A, Chang H, Sedough D, et al. Fabrication of controlled-release budesonide tablets via desktop (FDM) 3D printing. *Int J Pharm*. 2015;496(2):414–420. doi:10.1016/j.ijpharm.2015.10.039
35. Boraey MA, Hoe S, Sharif H, Miller DP, Lechuga-Ballesteros D, Vehring R. Improvement of the dispersibility of spray-dried budesonide powders using leucine in an ethanol–water cosolvent system. *Powder Technol*. 2013;236:171–178. doi:10.1016/j.powtec.2012.02.047

36. Mali AJ, Pawar AP, Purohit RN. Development of budesonide loaded biopolymer based dry powder inhaler: optimization, in vitro deposition, and cytotoxicity study. *J Pharm*. 2014;2014:12.
37. Sadeghi-Avalshahr A, Nokhasteh S, Molavi AM, Khorsand-Ghayeni M, Mahdavi-Shahri M. Synthesis and characterization of collagen/PLGA biodegradable skin scaffold fibers. *Regen Biomater*. 2017;4(5):309–314. doi:10.1093/rb/rbx026
38. da Silva FL, Ferreira HAL, de Souza AB, et al. Production of dulce de leche: the effect of starch addition. *LWT-Food Sci Technol*. 2015;62 (1):417–423. doi:10.1016/j.lwt.2014.10.062
39. Francisquini J, Pereira JPF, Pinto M, Carvalho AF, Perrone IT, Silva PH. Evolution of soluble solid content and evaporation rate curves during the manufacture of dulce de leche (dl). *Food Sci, Technol*. 2018;39:78–82. doi:10.1590/fst.26617
40. Zhang X, Zhao Z, Cui Y, et al. Effect of powder properties on the aerosolization performance of nanoporous mannitol particles as dry powder inhalation carriers. *Powder Technol*. 2019;358:46–54. doi:10.1016/j.powtec.2018.08.058
41. Kwon Y-B, Kang J-H, Han C-S, Kim D-W, Park C-W. The effect of particle size and surface roughness of spray-dried bosentan microparticles on aerodynamic performance for dry powder inhalation. *Pharmaceutics*. 2020;12(8):765. doi:10.3390/pharmaceutics12080765
42. Beratlis N, Balaras E, Squires K. Effects of dimples on laminar boundary layers. *J Turbul*. 2014;15(9):611–627. doi:10.1080/14685248.2014.918270
43. Hillery AM, Park K. *Drug Delivery: Fundamentals and Applications*. CRC Press; 2016.